AIAA JOURNAL
Vol. 34, No. 6, June 1996

Active Panel Flutter Suppression Using Self-Sensing Piezoactuators

F. Döngi,* D. Dinkler,† and B. Kröplin‡
University of Stuttgart, 70550 Stuttgart, Germany

Nonlinear flutter of flat and slightly curved panels in high supersonic flow is investigated based on a von Kármán plate model for the structure and on linear piston theory for aerodynamics. A finite element formulation of adaptive structures with piezoelectric material layers is developed using classical laminate theory. Sensor equations are derived for self-sensing piezoactuators. The paper briefly discusses linear and nonlinear flutter analysis techniques. Dynamic feedback control is used to suppress flutter of adaptive panels. Linear observer-based state feedback is shown to fail in the face of structural nonlinearity and flight parameter variations. Therefore, a novel control approach using output feedback from a pair of collocated or self-sensing piezoactuators is proposed. This new control methodology based on active compensation of aerodynamic stiffness terms is investigated regarding robustness and design limits.

Introduction

NONLINEAR panel flutter is known as a self-sustained oscillation occurring beyond a critical flight velocity in the high supersonic or hypersonic flow regime[1,2]; see Fig. 1. Because of aerodynamic pressure forces on the panel, two eigenmodes of the structure merge and lead to dynamic instability. The amplitudes of flutter motion are bounded because of tensile membrane stresses induced by bending of the geometrically nonlinear structure. Nevertheless, panel flutter should be avoided to prevent fatigue damage to the structure. The state of the art is to stiffen those panels in danger of flutter, a method that usually introduces additional weight to the design. In recent years, renewed interest in finite element-based investigations of nonlinear panel flutter has grown due to novel concepts of high-speed aircraft.[3,4] The use of adaptive materials such as shape memory alloys (SMAs) and piezoelectric ceramics has been proposed to save weight by actively suppressing panel flutter.[5–9] The approaches can be divided into static and dynamic actuation. Because of long heating/cooling cycles, SMA actuators are predestined for the static approach,[5] i.e., introducing a prestress field to the structure to increase the flutter boundary. Piezoceramic actuators were found to possess too low strain capability to be efficiently used in this way. However, dynamic feedback control with piezoelectric actuators has been investigated and shown to be able to suppress panel flutter.[6–9]

Lai et al.[6,7] and Zhou[8] use linear quadratic regulators (LQRs) for modal state feedback, which depends on measurements from modal sensors. However, it seems difficult to determine flight-state dependent aeroelastic modes using shaped sensors. In this paper, the application of a linear state observer is investigated. Alternatively, direct velocity feedback control has been applied to flutter suppression.[8,9] As will be pointed out here, this method is not efficient in the case of merged-mode flutter.

The paper first outlines the finite element formulation for the coupled electromechanical/aeroelastic problem of panels with piezoelectric material layers. Self-sensing actuators[10–12] as a special case of collocated actuator/sensor pairs are addressed. A brief survey of the LUM/NTF method[3,4] for nonlinear flutter analysis is given. State feedback control based on linear observers and a novel output feedback approach are then investigated using design examples of adaptive panels.

Received Jan. 13, 1995; presented as Paper 95-1078 at the AIAA/ASME Adaptive Structures Forum, New Orleans, LA, April 12–13, 1995; revision received July 14, 1995; accepted for publication July 14, 1995.

*Ph.D. Student, Institute for Statics and Dynamics of Aerospace Structures.

†Professor, Institute for Statics and Dynamics of Aerospace Structures, and Head, Aeroelasticity and Dynamics Group.

‡Professor and Head, Institute for Statics and Dynamics of Aerospace Structures.

Mathematical Model

Adaptive Panel Structure

The von Kármán plate equations including predeformations to allow for geometric imperfections are applied to model the structure. Using index notation, one can express the strains as follows:

$$\epsilon_{\alpha\beta} = \tfrac{1}{2}(v_{\alpha,\beta} + v_{\beta,\alpha}) + \tfrac{1}{2}(w_{,\alpha}w_{,\beta} + \bar{w}_{,\alpha}w_{,\beta} + w_{,\alpha}\bar{w}_{,\beta}) - x_3 w_{,\alpha\beta}$$
$$= \epsilon^0_{\alpha\beta} + x_3\kappa_{\alpha\beta} \qquad (\alpha, \beta = 1, 2) \tag{1}$$

where v_α, w, and $\kappa_{\alpha\beta}$ are the in-plane and transverse displacements and the curvature, respectively, and $\bar{w}$ denotes the transverse predeformation. The spatial coordinates are x_1, x_2, and x_3.

The adaptive panel is a composite structure with passive and active material layers; see Fig. 2. For passive material layers, stresses and strains are coupled via the elasticity tensor:

$$\sigma_{\alpha\beta} = E_{\alpha\beta\gamma\delta}\epsilon_{\gamma\delta} \tag{2}$$

Active layers are assumed to consist of piezoelectric materials that are polarized in the x_3 direction and isotropic in the $\{x_1, x_2\}$ plane. For this configuration the material law is given by

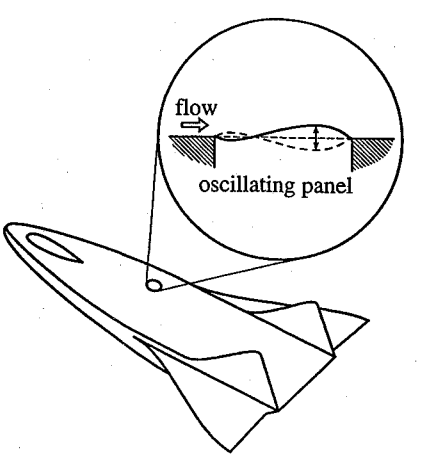

Fig. 1 Panel flutter at supersonic speeds.

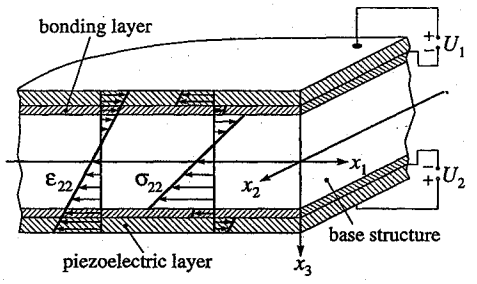

Fig. 2 Adaptive structure with piezoelectric layers.

$$\sigma_{\alpha\beta} = E_{\alpha\beta\gamma\delta}(\epsilon_{\gamma\delta} - d_{3\gamma\delta}\tilde{E}_3) \tag{3}$$

$$\tilde{D}_3 = \tilde{\epsilon}^*_{33}\tilde{E}_3 + d_{3\alpha\beta}E_{\alpha\beta\gamma\delta}\epsilon_{\gamma\delta}$$

where

$$\tilde{\epsilon}^*_{33} = \tilde{\epsilon}_{33} - d_{3\alpha\beta}E_{\alpha\beta\gamma\delta}d_{3\gamma\delta} \tag{4}$$

Here, $d_{\alpha\beta\gamma}$, $\tilde{E}_3$, $\tilde{\epsilon}_{33}$, and $\tilde{D}_3$ are the tensor of piezoelectric strain coefficients and the transverse components of the electric field, the electric permittivity, and the electric displacement, respectively. The electric field component is found by differentiation of the voltages across the layer thickness,

$$\tilde{E}_3 = -U_{,3} \tag{5}$$

A piezoelectric coupling tensor is defined as

$$\chi_{\alpha\beta} = E_{\alpha\beta\gamma\delta}d_{3\gamma\delta} \tag{6}$$

Consider a structure with n material layers, each of which has thickness $h_i (i = 1, \ldots, n)$. Let n_p layers be piezoelectric material layers denoted by indices $k(j)(j = 1, \ldots, n_p)$. Using classical laminate theory, one determines the stress resultants per unit length by integration across all layers:

$$n_{\alpha\beta} = \int_{(x_3)_0}^{(x_3)_n} \sigma_{\alpha\beta}\,dx_3 = A_{\alpha\beta\gamma\delta}\epsilon^0_{\gamma\delta} + B_{\alpha\beta\gamma\delta}\kappa_{\gamma\delta}$$

$$+ \sum_{j=1}^{n_p}(\chi_{\alpha\beta})_{k(j)}\int_{h_{k(j)}} U_{,3}\,dx_3 \tag{7}$$

$$m_{\alpha\beta} = \int_{(x_3)_0}^{(x_3)_n} \sigma_{\alpha\beta}x_3\,dx_3 = B_{\alpha\beta\gamma\delta}\epsilon^0_{\gamma\delta} + D_{\alpha\beta\gamma\delta}\kappa_{\gamma\delta}$$

$$+ \sum_{j=1}^{n_p}(\chi_{\alpha\beta})_{k(j)}\int_{h_{k(j)}} U_{,3}x_3\,dx_3 \tag{8}$$

The terms $A_{\alpha\beta\gamma\delta}$, $B_{\alpha\beta\gamma\delta}$, and $D_{\alpha\beta\gamma\delta}$ are the membrane, coupling, and bending stiffness tensors of the composite structure:

$$\langle A, B, D\rangle_{\alpha\beta\gamma\delta} = \int_{(x_3)_0}^{(x_3)_n} E_{\alpha\beta\gamma\delta}\langle 1, x_3, (x_3)^2\rangle\,dx_3 \tag{9}$$

Aerodynamic Loads

The aerodynamic model is based on inviscid, compressible potential flow. For the flight velocity region $\sqrt{2} < M_\infty < 6$, linear, quasistationary piston theory is applied to formulate the pressure loads on the panel[1–3,6–8]:

$$p^a_3 = \frac{\rho_\infty u^2_\infty}{\sqrt{M^2_\infty - 1}}\left[\frac{M^2_\infty - 2}{M^2_\infty - 1}\frac{w_{,t}}{u_\infty} + (\bar{w}_{,1} + w_{,1})\right] \tag{10}$$

where ρ_∞, u_∞, and M_∞ are the air density, flow velocity, and Mach number, respectively. The term $w_{,t}$ leads to aerodynamic damping, and $w_{,1}$ contributes to the stiffness of the aeroelastic system. Static aerodynamic loads occur in the case of panel predeformations.

Finite Element Formulation

The dynamic equilibrium of the coupled electromechanical/aeroelastic system is formulated in a weak form applying the principal of virtual work:

$$\delta W = \int_0^a\int_0^b \{\delta v_\alpha \mu v_{\alpha,tt} + \delta w \mu w_{,tt} - \delta v_{\alpha,\beta}n_{\alpha\beta}$$

$$+ \delta w_{,\alpha\beta}m_{\alpha\beta} - \delta w_{,\alpha}n_{\alpha\beta}(w + \bar{w})_{,\beta} + \delta v_\alpha p_\alpha + \delta w p_3$$

$$+ \delta w\frac{\rho_\infty u^2_\infty}{\sqrt{M^2_\infty - 1}}\left[\frac{M^2_\infty - 2}{M^2_\infty - 1}\frac{w_{,t}}{u_\infty} + (\bar{w}_{,1} + w_{,1})\right]dx_2\,dx_1$$

$$+ \sum_{j=1}^{N_p}\int_{V_{k(j)}} \delta U_{,3}\left\{\tilde{\epsilon}^*_{33}U_{,3} - (\chi_{\alpha\beta})_{k(j)}\epsilon_{\alpha\beta}\right\}dV_{k(j)}$$

$$+ \text{boundary terms} = 0 \tag{11}$$

Here, N_p denotes the total number of piezoelectric material patches in the structure, and p_α and p_3 are the in-plane and transverse loads per unit area, respectively. Integration of the virtual work is carried out across the plate dimensions a, b. The panel mass per unit area is determined by summing up the mass densities ρ_i of the layers:

$$\mu = \sum_{i=1}^{n}\rho_i h_i \tag{12}$$

To obtain nondimensional finite element matrices, Eq. (11) is multiplied by the factor $a^3/(D_0 b)$, where D_0 is the bending stiffness of a characteristic panel element to be defined for each design example. Furthermore, normalized spatial coordinates

$$\bar{x}_1 = x_1/a, \qquad \bar{x}_2 = x_2/b, \qquad \bar{x}_3 = x_3/h_0 \tag{13}$$

and a normalized time coordinate

$$\tau = \omega_0 t, \qquad \omega_0 = \sqrt{\frac{D_0}{\mu_0 a^4}} \tag{14}$$

are introduced using the mass per unit area μ_0 and thickness h_0 of the characteristic panel element. In the normalized formulation the virtual work due to the aerodynamic loads becomes

$$\int_0^1\int_0^1 \delta w[\sqrt{\lambda_a d_a}w_{,\tau} + \lambda_a(w_{,\bar{1}} + \bar{w}_{,\bar{1}})]\,d\bar{x}_2\,d\bar{x}_1 \tag{15}$$

where $w_{,\bar{1}}$ denotes differentiation with respect to $\bar{x}_1$. The nondimensional flow and aerodynamic damping parameters, respectively, are given by

$$\lambda_a = \frac{\rho_\infty u^2_\infty a^3}{\left(M^2_\infty - 1\right)^{0.5}D_0} \tag{16}$$

and

$$d_a = \frac{\left(M^2_\infty - 2\right)^2}{\left(M^2_\infty - 1\right)^{2.5}}\frac{\rho_\infty a}{\mu_0} \tag{17}$$

In the case of horizontal flight, λ_a and d_a are functions of the Mach number M_∞ only.

Substituting Eqs. (7) and (8) into expression (11) and considering the kinematic relationship (1), one obtains a formulation based on displacements and voltages. Spatial discretization is carried out using four-node rectangular finite elements with bilinear and bicubic Hermitian shape functions for in-plane and transverse displacements, respectively. Additionally, 12-node brick elements are used for each piezoelectric material layer. Interpolation of the voltages is chosen bilinear in the $\{x_1, x_2\}$ plane and biquadratic across the layer thickness. In reality, electrodes cover the top and bottom sides of the piezoelectric layers. As a consequence, the appropriate node voltages are set equal to each other. Zero potential levels are chosen at the bottom sides. The midplane variables remain free. For sensor layers this procedure leads to five DOFs per element. In the case of actuators the top node voltage is prescribed, which results in four DOFs per element.

Equations of Motion

After compilation of the element matrices, the equations of motion are found as

$$\begin{bmatrix} M_{dd} & 0 \\ 0 & 0 \end{bmatrix} q_{,\tau\tau} + \begin{bmatrix} D_{dd} & 0 \\ 0 & 0 \end{bmatrix} q_{,\tau} + \begin{bmatrix} K_{dd}(v,\bar{v}) & K_{de}(v,\bar{v}) \\ K_{ed}(v,\bar{v}) & K_{ee} \end{bmatrix} q = \begin{bmatrix} p_d \\ 0 \end{bmatrix} + \begin{bmatrix} F_d(v,\bar{v}) \\ F_e \end{bmatrix} \bar{U} \tag{18}$$

Here, the vector of DOFs is given by $q^T = [v^T U^T]$, where v and U are the vectors of node displacements and node voltages, respectively. The indices d and e denote terms coupling with displacements and electric voltages, respectively, and p_d is the vector of external mechanical forces. The voltages $\bar{U}$ applied at the actuators exert influences on mechanical and electrical DOFs described by the input matrices F_d and F_e, respectively. Nonlinearities occur in the stiffness and input matrices. The stiffness matrix is unsymmetric due to aerodynamic load contributions and electromechanical coupling.

The number of DOFs is reduced by elimination of the node voltages U. Solving the second line in Eq. (18) for U and substitution in the first line yields a reduced equation for the node displacements:

$$M_{dd} v_{,\tau\tau} + D_{dd} v_{,\tau} + K^*_{dd} v = p_d + F^*_d \bar{U} \tag{19}$$

with the modified nonlinear stiffness matrix

$$K^*_{dd} = K_{dd} - K_{de} K^{-1}_{ee} K_{ed} \tag{20}$$

and the modified nonlinear input matrix

$$F^*_d = F_d - K_{de} K^{-1}_{ee} F_e \tag{21}$$

Both matrices can be divided into sums of terms with different order of nonlinearity in v_α and w:

$$\begin{aligned} K^*_{dd} &= {}^0K^*_{dd} + {}^1K^*_{dd} + {}^2K^*_{dd} \\ {}^0K^*_{dd} &= {}^0K_{dd} + K^a_{dd} - {}^0K_{de}\,{}^0K^{-1}_{ee}\,{}^0K_{ed} \\ {}^1K^*_{dd} &= {}^1K_{dd} - {}^1K_{de}\,{}^0K^{-1}_{ee}\,{}^0K_{ed} - {}^0K_{de}\,{}^0K^{-1}_{ee}\,{}^1K_{ed} \\ {}^2K^*_{dd} &= {}^2K_{dd} - {}^1K_{de}\,{}^0K^{-1}_{ee}\,{}^1K_{ed} \end{aligned} \tag{22}$$

$$\begin{aligned} F^*_d &= {}^0F^*_d + {}^1F^*_d \\ {}^0F^*_d &= {}^0F_d - {}^0K_{de}\,{}^0K^{-1}_{ee} F_e \\ {}^1F^*_d &= {}^1F_d - {}^1K_{de}\,{}^0K^{-1}_{ee} F_e \end{aligned} \tag{23}$$

The left superscripts refer to the order of nonlinearity. The term K^a_{dd} is the unsymmetric aerodynamic stiffness matrix the elements of which depend linearly on the flow parameter λ_a.

Sensor Output Equations

Piezoelectric sensors exhibit electric surface charges $\tilde{Q}$ when strained. From the principle of virtual work for a sensor layer $k(j)$ an expression for the electric charge $\tilde{Q}$ is obtained under the assumption of zero electric potential at the lower surface:

$$-\tilde{Q} = \int_{V_{k(j)}} \delta U_{,3} \left\{ \bar{\epsilon}^*_{33} U_{,3} - (\chi_{\alpha\beta})_{k(j)} \epsilon_{\alpha\beta} \right\} \mathrm{d}V_{k(j)} \tag{24}$$

A discrete sensor output equation can be obtained by using the finite element method with the 12-node brick elements described earlier. For a structure with an arbitrary number of strain sensor outputs, this yields

$$y = \tilde{Q} = S(v,\bar{v}) v \tag{25}$$

where S is the nonlinear sensor output matrix.

The idea of self-sensing piezoelectric actuators has been proposed by various authors.[10–12] These devices, which are also called sensoriactuators, represent a special case of collocated actuator/sensor pairs. In practice, the difficulty lies in adaptively tuning self-sensing actuators to compensate for their feedthrough capacitance.[11]

Subsequently, ideal self-sensing actuators are assumed for which the linearized output and input matrices are related as follows:

$${}^0S = \alpha \left({}^0F^*_d \right)^T \tag{26}$$

The real constant α is equal to 1 in the present formulation. Note that for the nonlinear parts of S and F^*_d, the preceding equation does not hold.

Flutter Analysis

The homogeneous part of the equations of motion (19) is transformed into a nonlinear time-invariant state equation

$$x_{,\tau}(\tau) = A(x,\bar{x})\, x(\tau) \tag{27}$$

where $x^T = [v^T v^T_{,\tau}]$, $\bar{x}^T = [\bar{v}^T 0]$, and A is the nonlinear state matrix:

$$A(x,\bar{x}) = \begin{bmatrix} 0 & I \\ -M^{-1}_{dd} K^*_{dd}(x,\bar{x}) & -M^{-1}_{dd} D_{dd} \end{bmatrix} \tag{28}$$

Flutter boundaries can be determined by linear eigenvalue analysis of the state matrix A_L linearized about the static equilibrium state x_0 of the panel:

$$A_L(\bar{x}) = \frac{\partial}{\partial x} [A(x,\bar{x})x] \bigg|_{x=x_0} \tag{29}$$

The linearized state matrix is a function of the aerodynamic parameters λ_a and d_a defined in Eqs. (16) and (17), respectively. For nondimensional flutter analysis d_a is usually held constant such that the eigenvalues of A_L depend on λ_a only. The flow parameter is successively increased until two eigenvalues of A_L merge and one of them crosses the stability boundary into the right half of the complex plane. The flow parameter λ^{cr}_a for which this happens is called the linear flutter boundary of the system.

In the parameter region $\lambda_a > \lambda^{cr}_a$ limit-cycle flutter occurs. The investigations are restricted to the prebuckling region of the panel. Hence, higher periodic and chaotic oscillations are not looked upon. Numerical time integration to determine flutter amplitudes is often very costly. Therefore, iterative methods based on harmonic analysis have been developed for flutter amplitude computation. In this paper the linearized updated mode/nonlinear time function (LUM/NTF) approximation approach by Xue and Mei[3] and Gray and Mei[4] is applied. This method assumes a harmonic oscillation of the state variables:

$$x(\tau) = \hat{w}\, \hat{x} \cos \omega\tau \tag{30}$$

where $\hat{x}$ is a complex vector normalized such that $\hat{w}$ represents the amplitude of the maximum transverse deflection in limit-cycle flutter. Because of the nonlinearity of state equation (27) substitution of Eq. (30) leads to higher order cosine terms that are approximated as follows:

$$\cos^2 \omega\tau = \sqrt{\tfrac{1}{2} + \tfrac{1}{2} \cos 2\omega\tau} \cos \omega\tau \approx (1/\sqrt{2}) \cos \omega\tau$$

$$\cos^3 \omega\tau = \tfrac{1}{4}(3 \cos \omega\tau + \cos 3\omega\tau) \approx \tfrac{3}{4} \cos \omega\tau$$

The determination of flutter amplitudes is based on the eigenproblem of a state matrix

$$\tilde{A}(\bar{x}) = \begin{bmatrix} 0 & I \\ -M^{-1}_{dd} \tilde{K}(\bar{x}) & -M^{-1}_{dd} D_{dd} \end{bmatrix} \tag{31}$$

with the new stiffness

$$\tilde{K}(\bar{x}) = {}^0K^*_{dd} + (\hat{w}/\sqrt{2})\,{}^1K^*_{dd}(\hat{x},\bar{x}) + (3\hat{w}^2/4)\,{}^2K^*_{dd}(\hat{x}^2,\bar{x}) \tag{32}$$

using the terms of Eq. (22). The LUM/NTF algorithm consists of an inner and an outer loop. In the inner loop, the nonlinear eigenproblem for the state matrix A is solved iteratively by successive eigenmode analyses of $\tilde{A}$ and updates of $\hat{x}$ until convergence of the eigenvalues is reached. The outer loop consists of the search of a λ^{cr}_a

with both d_a and the flutter amplitude $\hat{w}$ prescribed. In this manner, one obtains pairs $\{\lambda_a^{cr}(\hat{w}), \hat{w}\}$ that define a flutter amplitude diagram.

The influence of static loads such as temperature stresses, pressure differentials, or static aerodynamic loads due to geometric imperfections is investigated in a precomputation step using the Newton–Raphson iterative solution scheme. In such cases terms due to static displacements must be included in the nonlinear stiffness matrices in Eq. (32).

State Feedback Control

Lai et al.[6,7] and Zhou[8] propose linear optimal control of a reduced modal system for flutter suppression of panels with piezoelectric sensors and actuators. They assume that the modal state variables are known for feedback. In practice, modal sensors or state observers must be applied to obtain measurements or estimates of the modal coordinates. It seems difficult to account for varying aeroelastic modes with shaped modal sensors. Therefore, the performance of observer-based modal state feedback is subsequently investigated for a design example.

Consider a one-dimensional, simply supported aluminum panel in horizontal flight at a height of 20 km ($\rho_\infty = 0.089$ kg/m^3 and $a_\infty = 295.1$ m/s). The panel dimensions are length $a = 1.2$ m, width $b = 1$ m, and thickness $h = 2.2$ mm. A lead zirconate titanate (PZT) layer of thickness $h_p = 0.2$ mm is ideally attached at the lower surface of the panel. It is divided in two self-sensing actuators of equal length $a/2 = 0.6$ m. The mechanical and electrical material properties of aluminum and PZT are given in Table 1.

The panel is discretized with 12 elements in longitudinal direction resulting in 35 DOFs. Using linear eigenmode analysis, one finds the flutter boundary for the uncontrolled panel to be $\lambda_a^{cr} = 337.1$, which is equivalent to $M_\infty^{cr} = 1.931$.

Using the linear quadratic Gaussian/loop transfer recovery (LQG/LTR) methodology[13] a feedback controller is designed to suppress flutter up to $M_\infty = 6.0$. First, the equations of motion (19) are linearized and transformed into modal space resulting in a system with 35 modes. A reduced system with the first six modes is used to design a linear optimal controller. Robustness recovery[13] is carried out to achieve a linear observer. The compensator is checked for linear stability robustness with an eigenvalue analysis of the closed-loop system with 35 modes.

To compare linear quadratic regulator (LQR) performance with LQG performance, the closed-loop system without observer is backtransformed into physical coordinates and simulated including structural nonlinearity. This approach implies linear input behavior of the actuators. Simulation results using a Runge–Kutta–Merson integration scheme are given in Fig. 3. Starting from limit-cycle flutter at $M_\infty = 6.0$, the LQR is activated at $t = 0.0$ and successfully suppresses flutter motion within 1.0 s.

Table 1 Material constants of aluminum and PZT

Property	Unit	Aluminum	PZT
E	N/m^2	7.0×10^{10}	6.3×10^{10}
ν	—	0.33	0.292
ρ	kg/m^3	2710	7600
$d_{311} = d_{322}$	m/V	—	1.9×10^{10}
$d_{312} = d_{321}$	m/V	—	0
$\tilde{\epsilon}_{33}$	As/Vm	—	1.5×10^{-8}

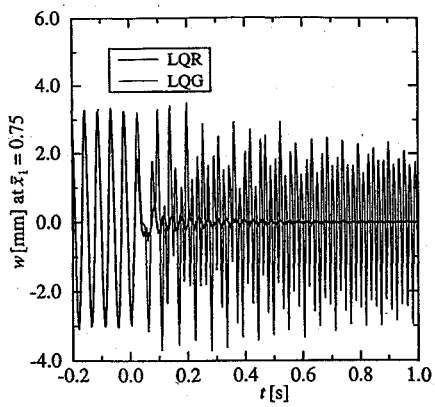

Fig. 3 Flutter suppression control: LQR vs LQG.

Numerical simulation of the LQG performance is carried out by coupling the nonlinear equations of motion with the modal observer equations via the nonlinear output matrix. The results are given in Fig. 3. The LQG compensator is found to be unable to meet the performance specifications of the LQR. This is due to the linear observer model that leads to incorrect estimation of modal states in the case of large nonlinear deflections of the panel. Note that to show this effect clearly actuator saturation was not considered for the simulations. Although the LQR designed for $M_\infty = 6.0$ yields stable closed-loop systems for all lower Mach numbers, LQG control is limited to the design case. Adaptation of observer parameters will be required if control for varying flight conditions is demanded.

The poor performance robustness was to be expected since a linear observer cannot efficiently simulate nonlinear structures. However, nonlinear observers proposed in the literature appear to be 1) not applicable to the distributed, high-dimensional system and 2) much too involved in the case of individual panel control under real flight conditions. To avoid the robustness problems of observer-based state feedback or the shape adaptivity requirements of modal sensors, output feedback control shall be investigated as an alternative approach.

ACAS Control

In the high supersonic range, merged-mode panel flutter is caused by nonconservative aerodynamic forces that are represented in the equations of motion (19) as skew-symmetric terms in the aerodynamic stiffness matrix $\boldsymbol{K}_{dd}^a$. The aerodynamic damping terms have a stabilizing effect on the panel dynamics. Their influence on the flutter boundary is small. Therefore, when aiming to suppress flutter with output feedback, it is pointless to put active damping into the system. This is different to the case of single mode flutter in the low supersonic range that is due to negative aerodynamic damping.[2] Frampton et al.[9] successfully used active damping to suppress panel flutter in this flow regime.

The idea of a controller for the active compensation of aerodynamic stiffness (ACAS) is outlined for an undamped two-mode system first. The aerodynamic stiffness matrix is not included in the eigenproblem but looked upon as a disturbance term. When transformed with the modal matrix of the undisturbed system, the modal aerodynamic stiffness matrix $\tilde{\boldsymbol{K}}^a$ is skew symmetric:

$$\begin{bmatrix} \tilde{v}_{1,\tau\tau} \\ \tilde{v}_{2,\tau\tau} \end{bmatrix} + \left\{ \begin{bmatrix} \omega_1^2 & 0 \\ 0 & \omega_2^2 \end{bmatrix} + \begin{bmatrix} 0 & +k \\ -k & 0 \end{bmatrix} \right\} \begin{bmatrix} \tilde{v}_1 \\ \tilde{v}_2 \end{bmatrix}$$

$$= \tilde{\boldsymbol{v}}_{,\tau\tau} + \{\boldsymbol{\Lambda} + \tilde{\boldsymbol{K}}^a\}\tilde{\boldsymbol{v}} = 0 \tag{33}$$

The squared eigenvalues of the disturbed system are

$$\lambda_{1,2}^2 = -\alpha_1 \pm \sqrt{\alpha_2^2 - k^2}$$

where

$$\alpha_1 = \frac{\omega_1^2 + \omega_2^2}{2}, \qquad \alpha_2 = \frac{\omega_2^2 - \omega_1^2}{2} \tag{34}$$

Dependent on the parameter $k \sim \lambda_a$, the eigenvalues take different locations in the complex plane; see Fig. 4.

Increasing k destabilizes the dynamic system. Hence, feedback control is chosen such that the influence of k is compensated.

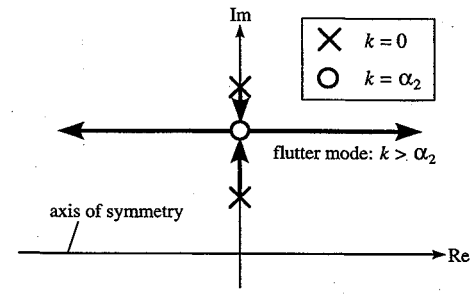

Fig. 4 Eigenvalues of disturbed system.

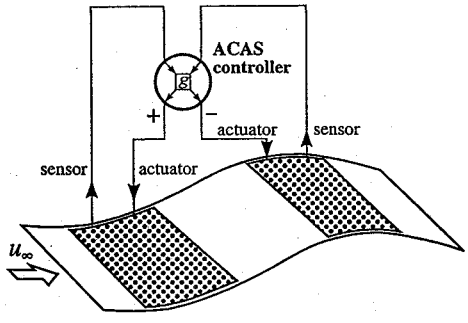

Fig. 5 ACAS control concept.

Consider the two-mode system to possess two self-sensing or collocated actuators the positions of which guarantee controllability. The linearized input and output matrices are transformed into modal space and inverted. Because of collocation, see Eq. (26), the modal inverse output and input matrices read

$$\tilde{S}^{-1} = \begin{bmatrix} c_{11} & c_{12} \\ c_{21} & c_{22} \end{bmatrix}, \qquad \tilde{F}^{-1} = \alpha \begin{bmatrix} c_{11} & c_{21} \\ c_{12} & c_{22} \end{bmatrix} \tag{35}$$

The control law for output feedback is chosen as follows:

$$\bar{U} = Gy, \qquad G = \gamma \tilde{F}^{-1} \tilde{K}^a \tilde{S}^{-1} \tag{36}$$

which leads to a skew-symmetric gain matrix, where $g = k\gamma\alpha(c_{11}c_{22} - c_{12}c_{21})$,

$$G = \begin{bmatrix} 0 & +g \\ -g & 0 \end{bmatrix} \tag{37}$$

Here, γ is a positive real tuning parameter. The closed-loop system contains a compensated modal aerodynamic stiffness matrix

$$\tilde{K}^a - \tilde{F}G\tilde{S} = (1-\gamma) \begin{bmatrix} 0 & +k \\ -k & 0 \end{bmatrix} \tag{38}$$

Thus, by applying ACAS control to a two-mode system, the parameter k is replaced by $(1-\gamma)k$. The skew symmetry of the gain matrix G implies that the output of the second self-sensing actuator is fed back to the first, and the output of the first actuator is fed back to the second, but with opposite sign of amplification; see Fig. 5.

For panels with an arbitrary number of modes ACAS control design must be slightly modified. First, an eigenmode analysis of the linearized, unperturbed system, i.e., without aerodynamic loads, is carried out. The structural matrices M and K, the input and output matrices F and S, and the aerodynamic stiffness matrix K^a are then transformed into modal space. The modal input and output matrices as well as the modal aerodynamic stiffness matrix are partitioned between the two merged modes and the remaining modes:

$$\tilde{F} = \begin{bmatrix} \tilde{F}_1 \\ \tilde{F}_2 \end{bmatrix}, \qquad \tilde{S} = \begin{bmatrix} \tilde{S}_1 & \tilde{S}_2 \end{bmatrix} \tag{39}$$

$$\tilde{K}^a = \begin{bmatrix} \tilde{K}^a_{11} & \tilde{K}^a_{12} \\ \tilde{K}^a_{21} & \tilde{K}^a_{22} \end{bmatrix} \tag{40}$$

The gain matrix for output feedback is chosen as

$$G = \gamma \tilde{F}_1^{-1} \tilde{K}^a_{11} \tilde{S}_1^{-1} \tag{41}$$

which yields the compensated modal aerodynamic stiffness matrix

$$\tilde{K}^a - \tilde{F}G\tilde{S} = \begin{bmatrix} (1-\gamma)\tilde{K}^a_{11} & \tilde{K}^a_{12} - \tilde{F}_1 G \tilde{S}_2 \\ \tilde{K}^a_{21} - \tilde{F}_2 G \tilde{S}_1 & \tilde{K}^a_{22} - \tilde{F}_2 G \tilde{S}_2 \end{bmatrix} \tag{42}$$

Again, compensation is achieved for the merged modes. However, dynamic spillover arises due to coupling terms in the remaining modes. The tuning parameter γ must be chosen such that both the merged modes are stabilized and the remaining eigenvalues stay in the complex left half-plane. These constraints put lower and upper bounds on γ.

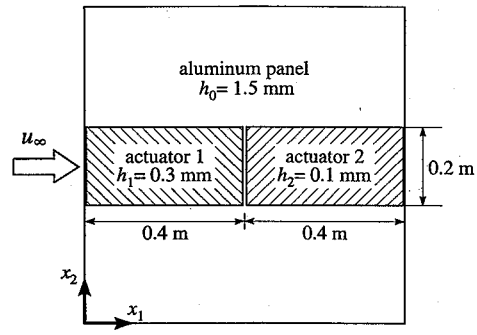

Fig. 6 Adaptive panel (bottom view).

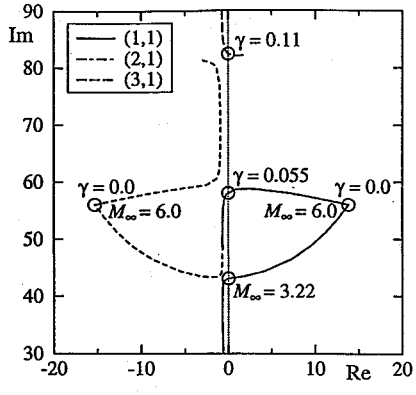

Fig. 7 Root loci during ACAS design process.

ACAS Design Example

The novel control concept is applied to a square, simply supported aluminum panel with a pair of self-sensing PZT actuators attached at the lower surface and exposed to supersonic flow at the upper surface; see Fig. 6. The material properties of aluminum and PZT are given in Table 1. Nondimensional computations are carried out using the characteristic properties h_0, μ_0, and D_0 of the aluminum layer. The panel is discretized with 8 × 8 finite elements leading to 322 mechanical DOFs. For horizontal flight at a height of 20 km the flutter boundary of the model is $M_\infty^{cr} = 3.22$. An ACAS controller shall be designed to suppress flutter up to $M_\infty = 6.0$. The mass savings compared with passive stabilization by increasing panel thickness amount to 15.9%.

Figure 7 shows the root loci of the plate modes (1, 1), (2, 1), and (3, 1) during the design process. The pair (m, n) denotes the numbers of half-waves in the flow (x_1) and the transverse (x_2) plate directions, respectively. First, the Mach number is increased from 2.0 to 6.0 for the uncontrolled system. Merging of modes (1, 1) and (2, 1) leads to instability for (1, 1) at $M_\infty = 3.22$. For constant $M_\infty = 6.0$ an ACAS controller is designed by increasing the tuning parameter γ from 0. At $\gamma_{min} = 0.055$ mode (1, 1) returns into the left half-plane. Dynamic spillover results in merging of modes (2, 1) and (3, 1) and instability at $\gamma_{max} = 0.11$. For the final design $\gamma = 0.06$ has been chosen.

The LUM/NTF algorithm has been extended to include the linear and nonlinear active stiffness matrices due to output feedback. For the uncontrolled and controlled design model, the results of LUM/NTF analyses are given in Fig. 8. The maximum flutter amplitudes shown here occur at $\bar{x}_1 = 0.75$, and $\bar{x}_2 = 0.5$. ACAS control increases the linear flutter boundary to $M_\infty = 6.67$. It is robust with respect to structural nonlinearity and Mach number or λ_a variations. However, physical performance limits exist: For the present model, actuator saturation occurs at $\bar{U}_1 = 180$ V at actuator 1. This value is reached for flutter with an amplitude of $\hat{w}/h_0 = 1.33$. It corresponds with the depolarization limit of the piezoelectric material at $\tilde{E}_{3\max} = 600$ V/mm.

Further robustness studies have been carried out considering static pressure differentials between upper and lower surface of the panel,

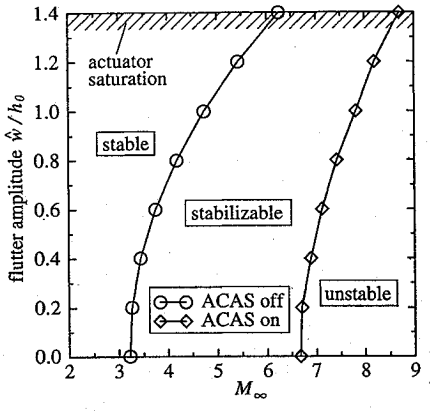

Fig. 8 Stability regions of the adaptive panel.

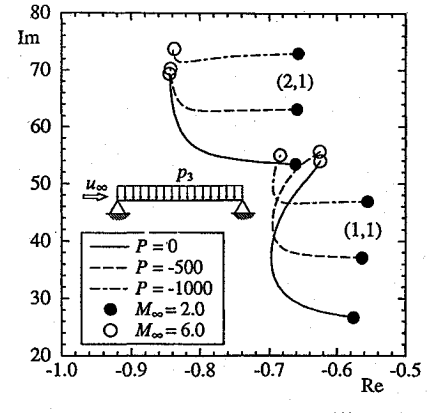

Fig. 9 Influence of static pressure differentials.

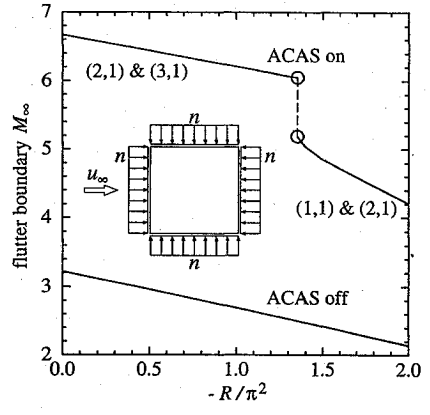

Fig. 10 Influence of static membrane loads.

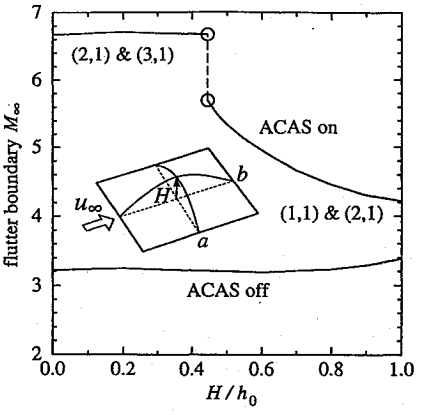

Fig. 11 Influence of geometric imperfections.

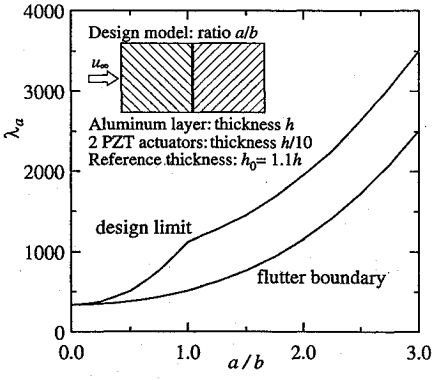

Fig. 12 ACAS design window.

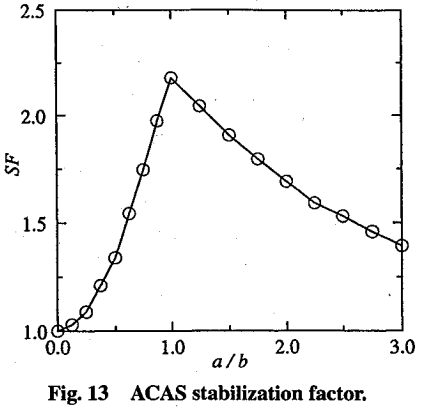

Fig. 13 ACAS stabilization factor.

static in-plane loads as they arise in case of temperature strains, and geometric imperfections such as curvature. Dowell[1,14] has investigated uncontrolled panels subject to those conditions. Static pressure differentials are found to increase the flutter boundary as do in-plane tensile loads. Both curvature and in-plane pressure loads, however, may significantly decrease the stability of panels in a flow.

An eigenmode analysis of the controlled panel subject to static pressure differentials and M_∞ variations shows that ACAS is robust in this case; see the root loci in Fig. 9. Here, the normalized pressure load is

$$P = \frac{p_3 a^4}{D_0 h_0} \tag{43}$$

For the panel with uniformly distributed in-plane pressure loads $n_{11} = n_{22} = n$, the normalized force is defined as

$$R = \left(na^2/D_0\right) \tag{44}$$

The square plate without actuators buckles at $R^{cr} = -2\pi^2$. Up to this value the flutter boundaries are given in Fig. 10. ACAS control exhibits poor robustness in this case. At $R/\pi^2 = -1.36$ merging of modes (1, 1) and (2, 1) significantly decreases the flutter boundary of the controlled system. Similar results are obtained in the case of geometric imperfections (see Fig. 11), where the predeformations have been chosen as

$$\bar{w} = -H\left[1 - \frac{(x_1 - a/2)^2}{(a/2)^2}\right]\left[1 - \frac{(x_2 - b/2)^2}{(b/2)^2}\right] \tag{45}$$

with H being the maximum predeformation in the middle of the panel.

ACAS Design Window

Dependent on the panel length to width ratio a/b, dynamic spillover can significantly limit the region $[\gamma_{min}, \gamma_{max}]$. The vanishing of $[\gamma_{min}, \gamma_{max}]$ defines a maximum controllable λ_a for each configuration. For rectangular panels with half/half actuators as given in Fig. 12 the design window for ACAS control is shown in the $\{a/b, \lambda_a\}$ parameter plane. It is bounded by the ACAS design limit λ_a^{max} and the passive flutter boundary λ_a^{cr}. The computations are based on the nondimensional formulation with a fixed damping parameter $d_a = 0.01$. An ACAS stabilization factor SF can be defined

by dividing the maximum controllable $\lambda_a^{\max}$ by the linear flutter boundary λ_a^{cr} of the uncontrolled panel. It is given in Fig. 13 whence follows that square panels are most attractive for ACAS control. Values of SF $\rightarrow$ 1 for high or low ratios of a/b signify that ACAS fails to rise the flutter boundary. In such cases ACAS performance might be enhanced by choosing the actuator/sensor placement to minimize spillover.

Conclusions

A finite element formulation for numerical investigations on adaptive panels with self-sensing piezoelectric actuators in high supersonic flow has been presented. Flutter analysis with the LUM/NTF approximation approach has been briefly outlined. When applied to suppress nonlinear panel flutter, state feedback based on linear observers exhibits very poor performance robustness. A novel control approach based on output feedback for active compensation of aerodynamic stiffness (ACAS) terms is proposed as an alternative. It is shown to possess good robustness properties regarding nonlinearity, flight parameter variations, and static pressure differentials. A further advantage is the simple feedback scheme that can be implemented with an analog circuit. In the case of static in-plane pressure loads or geometric imperfections, the performance of an ACAS controller may significantly deteriorate. An ACAS design window in dependence of panel geometry has been presented.

For future high-speed aircraft, both single-mode panel flutter in the low supersonic range and merged-mode flutter in the high supersonic and hypersonic range may occur. A combination of direct velocity feedback control and ACAS control could then present an efficient approach to flutter suppression. Future research work must include aerothermodynamics and the pyroelectric behavior of the actuator material.

Acknowledgment

This work has been financially supported by the Deutsche Forschungsgemeinschaft.

References

[1]Dowell, E. H., "Nonlinear Oscillations of a Fluttering Plate," *AIAA Journal*, Vol. 4, No. 7, 1966, pp. 1267–1275.

[2]Dowell, E. H., *Aeroelasticity of Plates and Shells*, Noordhoff International, Leyden, The Netherlands, 1975.

[3]Xue, D. Y., and Mei, C., "Finite Element Nonlinear Panel Flutter with Arbitrary Temperatures in Supersonic Flow," *AIAA Journal*, Vol. 31, No. 1, 1993, pp. 154–162.

[4]Gray, C. E., Jr., and Mei, C., "Large-Amplitude Finite Element Flutter Analysis of Composite Panels in Hypersonic Flow," *Proceedings of the AIAA/ASME/ASCE/AHS/ASC 33rd Structures, Structural Dynamics, and Materials Conference* (Dallas, TX), AIAA, Washington, DC, 1992, pp. 492–512.

[5]Weisshaar, T. A., and Sadlowski, M., "Panel Flutter Suppression with Active Microactuators," *Proceedings of the AAAF International Forum on Aeroelasticity and Structural Dynamics* (Strasbourg, France), AAAF, Paris, 1993, pp. 118–129.

[6]Lai, Z., Zhou, R. C., Xue, D. Y., Huang, J.-K., and Mei, C., "Suppression of Nonlinear Panel Flutter at Elevated Temperature with Piezoelectric Actuators," *Proceedings of the AIAA/ASME/ASCE/AHS/ASC 34th Structures, Structural Dynamics, and Materials Conference* (La Jolla, CA), AIAA, Washington, DC, 1993, pp. 3466–3474.

[7]Lai, Z., Xue, D. Y., Huang, J.-K., and Mei, C., "Panel Flutter Limit-Cycle Suppression with Piezoelectric Actuation," *Journal of Intelligent Material Systems and Structures*, Vol. 6, No. 2, 1995, pp. 274–282.

[8]Zhou, R. C., "Suppression of Nonlinear Flutter of Composite Panels at Supersonic Speeds and Elevated Temperatures," *Proceedings of the AIAA/ASME/ASCE/AHS/ASC 36th Structures, Structural Dynamics, and Materials Conference* (New Orleans, LA), AIAA, Washington, DC, 1995, pp. 288–298.

[9]Frampton, K. D., Clark, R. L., and Dowell, E. H., "Active Control of Panel Flutter with Linearized Potential Flow Aerodynamics," *Proceedings of the AIAA/ASME/ASCE/AHS/ASC 36th Structures, Structural Dynamics, and Materials Conference* (New Orleans, LA), AIAA, Washington, DC, 1995, pp. 2273–2280.

[10]Anderson, E. H., Hagood, N. W., and Goodliffe, J. M., "Self-Sensing Piezoelectric Actuation: Analysis and Application to Controlled Structures," *Proceedings of the AIAA/ASME/ASCE/AHS/ASC 33rd Structures, Structural Dynamics, and Materials Conference* (Dallas, TX), AIAA, Washington, DC, 1992, pp. 2141–2155.

[11]Cole, D. G., and Clark, R. L., "Adaptive Compensation of Piezoelectric Sensoriactuators," *Journal of Intelligent Material Systems and Structures*, Vol. 5, Sept. 1994, pp. 665–672.

[12]Dosch, J. J., Inman, D. J., and Garcia, E., "A Self-Sensing Piezoelectric Actuator for Collocated Control," *Journal of Intelligent Material Systems and Structures*, Vol. 3, Jan. 1992, pp. 166–185.

[13]Doyle, J. C., and Stein, G., "Multivariable Feedback Design: Concepts for a Classical/Modern Synthesis," *IEEE Transactions on Automatic Control*, Vol. AC-26, No. 1, 1981, pp. 4–16.

[14]Dowell, E. H., "Nonlinear Flutter of Curved Plates," *AIAA Journal*, Vol. 7, No. 3, 1969, pp. 424–431.